Multi-Objective Optimized Operation of Energy Storage Devices

Bart Homan
dept. of EEMCS
University of Twente
Enschede, the Netherlands
b.homan@utwente.nl

Gerwin Hoogsteen
dept. of EEMCS
University of Twente
Enschede, the Netherlands
g.hoogsteen@utwente.nl

Johann Hurink
dept. of EEMCS
University of Twente
Enschede, the Netherlands
j.l.hurink@utwente.nl

***Abstract*—In this work, we present a novel modular approach for control of an energy storage device towards multiple objectives simultaneously. The proposed control method is explained and its usefulness is demonstrated using simulations of a 16 house neighbourhood. The simulation results of the proposed approach are compared to those using a standard battery setup. It is concluded that, when a storage device is divided in *virtual storage devices*, which each have their own goal (e.g. peak-shaving, grid-balancing and economic benefits in energy markets) and their own (dedicated) fraction of the storage device capacity, improvements in storage device utilization can be achieved.**

***Index Terms*—Energy storage, Optimization, Multi-objective operation, Control strategy**

I. Introduction

Energy storage devices can be deployed for various applications, like e.g. peak-shaving, load-shifting (energy management) and grid frequency stabilization (power management). Each of these applications requires the energy storage device to operate on different time-scales, steering signals and under different conditions. However, the use of a storage device for only one application often results in underutilization of the storage asset, resulting in reduced (financial) benefits and unprofitable business cases [1], [2], thereby preventing storage from being deployed at all.

In this paper we introduce a novel approach to optimize the operation of one energy storage device in a way that optimizes its operation towards multiple objectives simultaneously. In the proposed control strategy we split up the storage device in multiple virtual storage devices (*VSD*s). Each of these VSDs can be controlled and optimized by its own application specific controller, enabling the use of existing device models and optimization algorithms. To integrate the different VSDs, they are governed by one over-all controller, which ensures that there is one over-all result for the combined VSDs.

This paper is structured as follows. In Section II the proposed multi-objective control strategy is presented. In Section III the simulation setup used to demonstrate the control strategy is introduced, followed in Section IV by a discussion of the results, and in Section V by our conclusions.

II. Multi-objective control strategy

In the proposed control strategy we consider an actual storage device (*ASD*), e.g. a battery or super-capacitor, with a given capacity C (represented by the blue square in Fig. 1). This ASD is divided into n virtual storage devices *VSD*$_i$, $i \in \{1, 2, ..., n\}$ (represented by the dashed blue squares in Fig. 1). Each VSD$_i$ has its own operational constraints, application-specific objectives and optimization approach (e.g. a (dis)charge power or (dis)charge time regime). Furthermore, for each VSD$_i$ a different device model can be used to control the storage device (for example VSD$_1$ could be modelled as a non-ideal battery using the DiBu-model [3], while VSD$_2$ could be modelled as an ideal battery using the coulomb counting method [4]). Finally, each VSD$_i$ has its own capacity C_i and charge/discharge power.

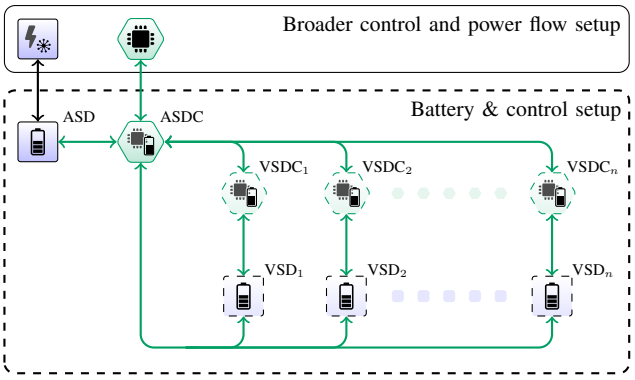

Fig. 1. Schematic representation of the proposed storage device control. Blue squares represent devices and green hexagons represent control algorithms.

Note, that in this control strategy the sum of the capacities C_i of all VSD$_i$s may be larger than the capacity C of the ASD. The reason for this is that in practice the probability of all VSDs to be at their upper capacity limits is expected to be small. Hence, allowing $\sum_{i=1}^{n} C_i > C$ may support a better utilization of the ASD.

For each VSD$_i$ there is a controller *VSDC*$_i$ (represented by a dashed green hexagon in Fig. 1). This VSDC$_i$ optimizes and plans the operation of the virtual storage device for each time-interval, i.e. it decides when and with how much power to charge or discharge the VSD$_i$. Using discretization of the planning horizon into m discrete time intervals, this results in a vector of planned power setpoints $\vec{x}_i = [x_{i,1}, x_{i,2}, \ldots, x_{i,m}]$. As such, the control and optimization of the virtual storage device can be handled in the same way as the operation of actual storage devices. In this paper we use the algorithms and models implemented in DEMKit [5] for this.

The desired (dis)charging power $x_{i,t}$ of VSD$_i$ at a given time t, determined by VSDC$_i$ is then communicated to the actual storage device controller (*ASDC*). The ASDC, represented by

978-1-6654-4875-8/21/$31.00 ©2021 IEEE

2021 IEEE PES Innovative Smart Grid Technologies Europe (ISGT Europe) | 978-1-6654-4875-8/21/$31.00 ©2021 IEEE | DOI: 10.1109/ISGTEUROPE52324.2021.9640150

the green hexagon in Fig. 1, controls the (dis)charge power of the ASD by aggregating the desired powers $x_{i,t}$ of all VSDs. Since the sum of capacities or power ratings of all VSDs may surpass the capacity and/or power rating of the ASD, an additional control loop is implemented in the ASDC to determine feasible control actions for the ASD. This loop has to ensure that the control action is feasible with respect to the SoC, capacity, and power constraints of the ASD. To achieve this, we have chosen to implement a prioritization of the VSDs using a priority list. This prioritization is based on the numbering of the VSDs, where a lower index means a higher priority, i.e. $\text{VSD}_1 > \text{VSD}_2 > \cdots > \text{VSD}_n$. This implies that the highest priority should be given to apply the desired power $\vec{x}_{1,t}$ for VSD_1, followed by the the desired power for VSD_2 and so on. For this, the ASDC first checks if $P^- \leq \sum_{i=1}^{n} \vec{x}_{i,t} \leq P^+$, where $P^- < 0$ and $P^+ > 0$ denote the maximum discharge and charge power of the ASD respectively. Similarly, the ASDC also checks whether the resulting control fits within the physical storage capacity constraints of the ASD, i.e. the stored energy is between 0 and the ASD capacity. If both are true, the desired aggregated power of all VSDs is communicated to the ASD. If not true, the prioritization is used to adapt the aggregated planned power profile. This happens in a way such that the difference between the desired power of a VSD and a feasible power to be charged/discharged, is minimized in a best possible way using the prioritization.

This best allocation is based on the feasible subset X of desired (dis)charge power values that still fit within aforementioned constraints of the ASD. Let $x_{\text{ASD},t} = \sum_{x \in X} x$ denote the aggregated power that is applied to the ASD. We determine the set X by iteratively adding the next prioritized planned power value $x_{i,t}$ to X as long as this results in a feasible solution. In practice, this means that the planned power of the VSDs with highest priorities can still be executed, but that in some cases adaptations may be required for lower prioritized VSDs. For example, if for three charging VSDs we have $x_{1,t} + x_{2,t} < P^+$ but $x_{1,t} + x_{2,t} + x_{3,t} > P^+$. In this case, the values $x_{1,t}$ and $x_{2,t}$ can be fully executed, but $x_{3,t}$ not, resulting in $X = \{x_{1,t}, x_{2,t}\}$.

If VSD_j is the next prioritized VSD that is not fully feasible within the ASD constraints (in the above case VSD_3), we calculate the best effort power $x_{j',t}$. We obtain $x_{j',t}$ by minimizing $|x_{j,t} - x_{j',t}|$ while ensuring that $x_{\text{ASD},t}$ still satisfies the constraints of the ASD when including $x_{j',t}$ in X. This means in practice that the ASD will be operated at its limits, i.e. full charging power $x_{\text{ASD},t} = P^+$, or full discharging power $x_{\text{ASD},t} = P^-$, or within its capacity constraints otherwise. The adapted value $x_{j',t}$ is then included in X.

We continue to iterate as it may be that the desired $x_{k,t}$ of an even lower prioritized VSD_k is feasible, e.g., when the ASD is to charge at full power ($x_{\text{ASD},t} = P^+$) but VSD_k desires to discharge ($x_{k,t} < 0$) or vice versa. In this case $x_{k,t}$ is added to X and a new iteration is started. In this new iteration we check again if a higher prioritized VSD_j can be served better now, i.e. by further minimizing $|x_{j,t} - x_{j',t}|$. These allocation iterations are performed until there is no improvement possible. In the example, this may be the case when we add a fourth VSD, such that $P^- \leq x_{1,t} + x_{2,t} + x_{3,t} + x_{4,t} \leq P^+$. In this case $x_{4,t}$ can be added to X, and in the next iteration it becomes clear that $x_{3,t}$ can also be fully executed, meaning that $x_{3',t}$ is replaced by $x_{3,t}$ in X.

Note, that the desired power ($x_{i,t}$) for the different VSDs can be contradictory, e.g. desired power $x_{1,t}$ may require VSD_1 to be discharged, while desired power $x_{2,t}$ requires VSD_2 to be charged. However, this always results in one over-all objective power ($x_{\text{ASD},t}$) for the ASD. Note, that this is also the net result one would obtain when two separate ESSs are used. Hence, the ASD always performs only one operation (i.e. charging, discharging or idle) at a time.

III. Simulation Setup

To demonstrate the multi-objective control strategy, a simulation of a 16 house neighbourhood microgrid, sharing one central energy storage device, is used. In this section the details of the simulated neighbourhood and the details of the battery & control setup are discussed.

A. Neighbourhood setup

The simulation setup of the neighbourhood has been adapted from [6]. Unless specifically stated, in the following the settings and parameters used in [6] are maintained. A schematic representation of the power flow and control structure of the neighbourhood is given in Fig. 2.

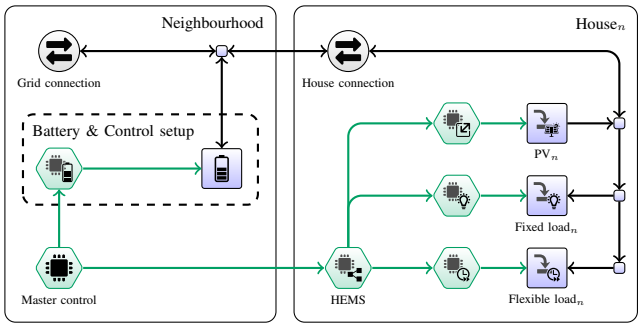

Fig. 2. Schematic representation of the simulated neighbourhood. Blue squares represent devices and green hexagons represent control algorithms.

The considered 16 house neighbourhood is arranged around a square with four houses on each side. The houses on the north and south side of the square each have a total surface of 19.2 m^2 roof mounted PV-panels (16% efficiency) facing south, while the houses on the east and west side of the square have the same amount of PV-panels facing west and east respectively. Each house has both fixed and flexible loads. The load profiles for these loads have been generated using the *Artificial Load Profile Generator* (ALPG) [7], taking into account various types of residents. The neighbourhood shares one connection to the main grid, with a limited capacity of 16 kW. The neighbourhood also shares one 200 kWh battery, with a (dis)charge power of 200 kW. The battery is primarily used to keep the grid exchange of the neighbourhood microgrid below the $\pm$16 kW limit.

In Fig. 3 the power profile for the neighbourhood, resulting from aggregation of the profiles for the fixed and flexible loads (generated using the ALPG) and the PV production for all 16 houses, is displayed. Note, that this power profile is generated for one week during the summer (July 11-18), which is sufficient for the demonstration of the proposed control strategy. For a more detailed demonstration of the ALPG (including seasonal influences) and of the application of generated profiles see [6], [7].

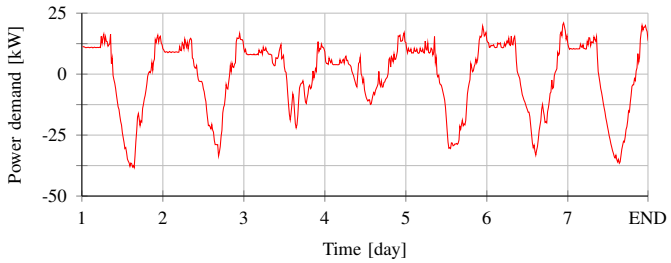

Fig. 3. Aggregated power profile for the 16 house neighbourhood. Note, that positive numbers indicate load, negative numbers indicate production.

B. Battery & control setup

The battery and control setup presented in the dashed rectangle in Fig. 2, represents the *Standard Battery* (SB) setup. This setup uses one battery (represented by the blue square) and one battery controller (represented by the green hexagon). The battery is modelled as an ideal battery and the battery controller can optimize the battery behaviour towards one objective. For the simulations where the multi-objective control strategy, introduced in this paper, is applied, this part of the neighbourhood model is replaced by the battery and control setup presented in Fig. 1; this case is referred to as the *Virtual Battery* (VB) setup. Note, that also in this setup the ASD and VSDs are modelled as ideal batteries. For both setups four different battery controllers are used:

1) PS control: The peak-shaving battery control has the goal of using the battery to minimize the exchange between the neighbourhood microgrid and the grid. This goal is pursued by coordinating the energy profile of the neighbourhood using the profile steering algorithm [8]. Here, a planning of the energy usage for m intervals in the future is made using predictions of the load profiles and weather forecasts. The optimization objective is to minimize $||\vec{x}||_2$, where $\vec{x} = [\vec{x}_1, \vec{x}_2, \ldots, \vec{x}_m]$ represents the planned grid exchange of the microgrid. This planning is then executed, and updated using partial replanning when either the predictions are updated or the current planning becomes infeasible due to prediction errors [9]. In this work we plan two days ahead and use discrete intervals of 15 minutes each, leading to $m = 192$.

2) BB control: The balancing battery control is an extension to the PS control approach. It has the goal of using the battery to react in real-time to observed peaks and dips in the microgrid exchange by allowing slight deviations from the created battery planning $\vec{x}_{\text{bat}}$. Here, the goal is to control the battery such that the real-time power exchange of the microgrid is maintained at the planned overall microgrid profile $\vec{x}$, instead of $\vec{x}_{\text{bat}}$ as used in PS control. A new battery optimization is executed when the actual operation of the battery deviates too much from the planning.

3) BB-NP control: The balancing battery without planning strategy is a pure real-time strategy that controls the battery power to maintain the grid exchange at a preconfigured value whenever possible, based on measurements. Within this work, we use a static grid exchange setpoint of 0.

4) APX control: The APX battery control has the goal of maximizing the profit based on the passive imbalance market prices of the APX market [10]. Again, we use a planning horizon of $m = 192$ intervals of 15 minutes each. Furthermore, perfect knowledge of future market prices is assumed.

IV. Simulation results

In this section, the simulation results of the 16 house neighbourhood with various battery controllers, during one week in the summer, are discussed.

A. Standard battery setup

In Fig. 4 the simulations of the total grid exchange for the neighbourhood, using the SB setup are presented for each of the battery controllers. Detailed results for the simulations presented in Fig. 4 are summarised in Table I.

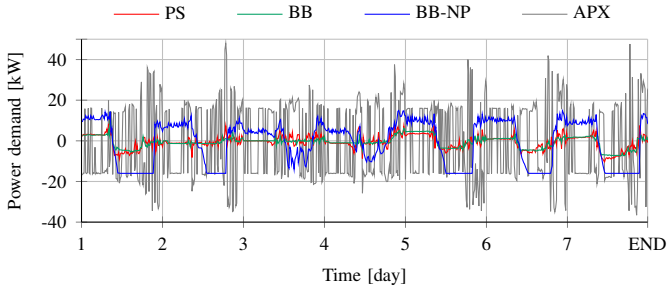

Fig. 4. Grid exchange for the neighbourhood, using the SB setup and using various battery controllers. Note, that positive numbers indicate imports from the grid, negative numbers indicate exports to the grid.

In the PS and BB cases the grid exchange is limited; in both cases the largest exchange is an import to the neighbourhood of 11 kW and 14 kW, respectively, successfully keeping the grid exchange within the $\pm$16 kW limit. As expected, the BB battery control leads to the smoothest grid exchange profile, as it uses both a planning and active response to peaks in the grid. The resulting grid exchanges can be considered grid-friendly. In the BB-NP case, the grid exchange is still limited, but in several time intervals the $\pm$16 kW limit is violated when electricity is exported to the grid. This occurs because at these times the battery is already completely charged due to excess electricity production in the neighbourhood. In the APX case there are large exchanges with the grid, surpassing the $\pm$16 kW limit in many time intervals. The largest exchange is an import of 48 kW. The battery is operated to maximize profit on the APX market, leading to an earning of €395 in this week, neglecting costs associated with frequent grid overloading and capacity violation.

TABLE I
Total grid exchange for the neighbourhood using the SB setup, calculated from the results presented in Fig. 4.

	PS	**BB**	**BB-NP**	**APX**
$\|\|\vec{x}\|\|_2$ $[kW]$	$7.77{\cdot}10^6$	$5.84{\cdot}10^6$	$7.85{\cdot}10^7$	$2.50{\cdot}10^8$
$max\ \|x_t\| \in \vec{x}$ $[kW]$	11	14	16	48

B. Virtual battery setup (PS-cases)

For the simulations using the VB setup, we consider simulations of cases where two VSDs are used (i.e. $n = 2$) and where $\sum_{i=1}^{n} C_i = C$. In each simulation the full ASD capacity is available, where for each simulation the percentage of capacity assigned to VSD_2 is given, while the remaining capacity is assigned to VSD_1. Detailed results for the simulations presented in Fig. 5, 6, 7 and 8 are summarised in Table II.

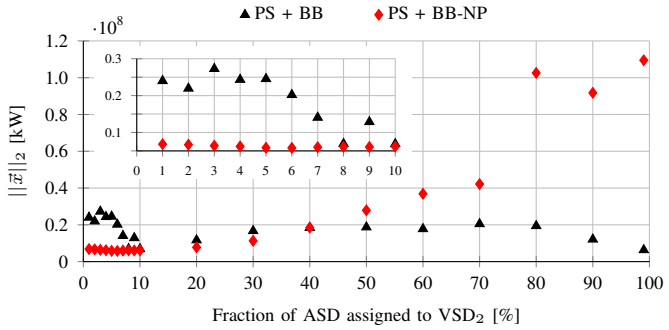

Fig. 5. Total grid exchange from simulations using the VB setup.

In Fig. 5 the total absolute grid exchange during the simulated week, calculated from simulations where VSD_1 uses PS battery control and VSD_2 uses either BB or BB-NP battery control, are presented.

In the PS + BB case (see Fig. 5), the total grid exchange does not vary much when the capacity of VSD_2 (i.e. the fraction of the ASD used for BB control) is increased. Most notably, the total grid exchange decreases when the VSD_2 capacity is increased from 1% to 10% (see Fig. 5 inlay). Between 10% and 100% there are only minor variations in grid exchange, with a local maximum at 70%. The smallest total grid exchange occurs at 99% of the ASD capacity assigned to VSD_2, this is comparable to the total grid exchange of the PS and BB cases in the SB setup (see Table I). The absence of large variations in the total grid exchange, and the lack of clear improvements with respect to the corresponding control in the SB setup, is attributed to the fact that the BB battery control already incorporates similar elements of both planning and real-time adjustments.

In the PS + BB-NP case the total grid exchange increases as the fraction of ASD assigned to VSD_2 increases. This is expected, because increasing the part of the ASD that is used to react on (random) occurrences in the grid, also increases the likelihood that the ASC is nearly empty or full when it needs to react, which implies that no reaction can take place. Hence, more severe grid exchanges are likely to take place when the capacity of VSD_2 is larger. Notably, the total grid exchange in the PS + BB-NP case is smaller than that of the SB setup using the PS or BB-NP cases, when the fraction of VSD_2 is between 1% and 20%. When this fraction is between 5% and 6% the total grid exchange is also smaller than in the SB setup, using the BB case. Hence, using these fractions of PS and BB-NP controlled VSDs in the VB setup, is a slight improvement with respect to using PS, BB or BB-NP control in the SB setup.

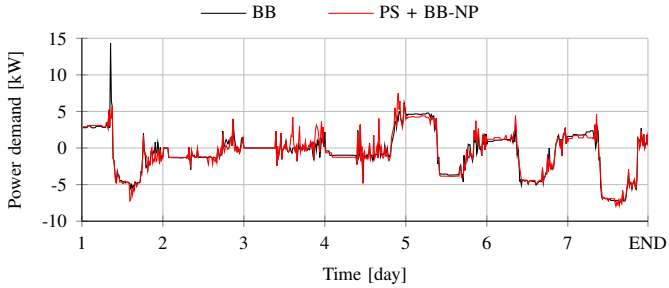

Fig. 6. Grid exchange for the neighbourhood, using SB setup with BB case and VB setup with PS + BB-NP (5%) case. Note, that positive numbers indicate imports from the grid, negative numbers indicate exports to the grid.

In Fig. 6 the grid exchange of a simulation using the SB setup and BB case is compared to that of a simulation using the VB setup and the PS + BB-NP case, where 5% of the ASD capacity is assigned to VSD_2. The resulting grid exchange profiles are very similar. On the one hand, the profile for the BB case is smoother, but on the other hand the total grid exchange for the PS + BB-NP case is lower. In both cases the grid exchange always remains within the ± 16 kW limit.

C. Virtual battery setup (APX-cases)

In this Subsection we discuss cases where where VSD_1 uses APX battery control and VSD_2 uses either PS or BB-NP battery control. In Fig. 7a the total grid exchange of these cases is presented, while in Fig. 7b the *theoretical* earnings on the APX market are presented. Note, that the penalties of grid overloading are not taken into account.

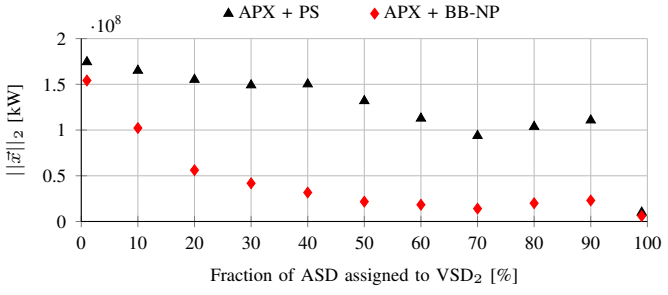

(a) Total grid exchange

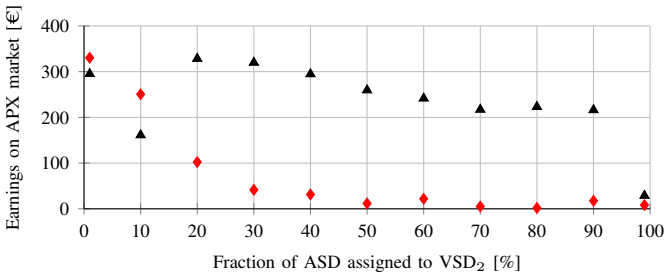

(b) Earnings on APX market

Fig. 7. Total grid exchange (a) and theoretical earnings on the APX market (b) calculated from simulations using the VB setup.

In the APX + PS case, the total grid exchange is high, even when 90% of the fraction of ASD capacity is assigned to VSD_2. Only when very small fractions of the ASD capacity are assigned to VSD_1, (i.e. with the goal to make profit on the APX market), the grid exchanges are significantly decreased. However, over-all the grid exchange is lower than that of the SB setup using the APX case, hence, an improvement on grid exchanges is observed. The earnings on the APX market are also rather consistent, in most cases a total of over €200,- is earned over the week, with a maximum of €328,- when 20% of the ASD capacity is assigned to VSD_2. Hence, by considering both applications, improvements can be made to the utilization of the battery.

TABLE II
TOTAL GRID EXCHANGE FOR THE NEIGHBOURHOOD USING THE VB SETUP. NOTE, THAT THE PERCENTAGE OF CAPACITY ASSIGNED TO VSD_2 IS GIVEN AND THE REMAINING CAPACITY IS ASSIGNED TO VSD_1.

VSD_2 (%)	1	10	20	30	40	50	60	70	80	90	99
	$\|\|\vec{x}\|\|_2$ $[kW]$										
PS + BB	$2.4{\cdot}10^7$	$6.9{\cdot}10^6$	$1.2{\cdot}10^7$	$1.7{\cdot}10^7$	$1.8{\cdot}\ 10^7$	$1.9{\cdot}10^7$	$1.8{\cdot}\ 10^7$	$2.0{\cdot}\ 10^7$	$1.9{\cdot}\ 10^7$	$1.2{\cdot}\ 10^7$	$\mathbf{6.3{\cdot}\ 10^6}$
PS + BB-NP	$6.8{\cdot}10^6$	$\mathbf{6.2{\cdot}10^6}$	$7.8{\cdot}10^6$	$1.1{\cdot}10^7$	$1.9{\cdot}\ 10^7$	$2.8{\cdot}10^7$	$3.7{\cdot}\ 10^7$	$4.2{\cdot}\ 10^7$	$1.0{\cdot}\ 10^8$	$9.2{\cdot}\ 10^7$	$1.1{\cdot}\ 10^8$
APX + PS	$1.7{\cdot}10^8$	$1.7{\cdot}10^8$	$1.6{\cdot}10^8$	$1.5{\cdot}10^8$	$1.5{\cdot}\ 10^8$	$1.3{\cdot}10^8$	$1.1{\cdot}\ 10^8$	$9.4{\cdot}\ 10^7$	$1.0{\cdot}\ 10^8$	$1.1{\cdot}\ 10^8$	$\mathbf{9.9{\cdot}\ 10^6}$
APX + BB-NP	$1.5{\cdot}10^8$	$1.0{\cdot}10^8$	$5.6{\cdot}10^7$	$4.2{\cdot}10^7$	$3.2{\cdot}\ 10^7$	$2.2{\cdot}10^7$	$1.8{\cdot}\ 10^7$	$1.4{\cdot}\ 10^7$	$2.0{\cdot}\ 10^7$	$2.3{\cdot}\ 10^7$	$\mathbf{6.0{\cdot}\ 10^6}$
	$max\ \|x_t\| \in \vec{x}$ $[kW]$										
PS + BB	16	12	14	16	16	16	15	16	16	16	**21**
PS + BB-NP	10	8	9	11	15	16	16	16	**40**	**38**	**37**
APX + PS	**37**	**38**	**28**	**26**	**37**	16	16	16	16	16	11
APX + BB-NP	16	16	16	16	16	16	16	16	16	16	11
	Earnings on the APX market [€]										
APX + PS	295	161	**328**	320	295	259	242	217	223	216	29
APX + BB-NP	**330**	251	102	41	31	12	22	5	2	17	8

In the APX + BB-NP case, both the total grid exchange and the earnings on the APX market decrease as the fraction of the ASD capacity assigned to VSD_2 increases. The explanation for this is that the APX control is countered by the BB-NP control due to conflicting objectives; exchange maximization vs. minimization respectively. The larger the part of the ASD gets, that is assigned to VSD_2, the more effective this countering becomes. Hence, combinations of the APX and BB-NP controls yield no improvements.

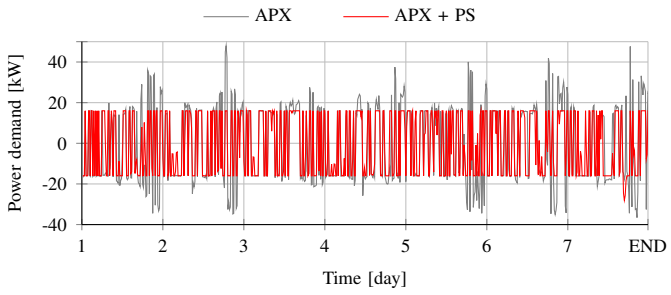

Fig. 8. Grid exchange for the neighbourhood, using SB setup with APX case and VB setup with APX + PS (20%) case. Note, that positive numbers indicate imports from the grid, negative numbers indicate exports to the grid.

In Fig. 8 the grid exchange of a simulation using the SB setup with APX case is compared to that of a simulation using the VB setup with APX + PS case, where 20% of the ASD capacity is assigned to VSD_2. In the APX case, €395,- is earned on the APX market, however, the grid exchange regularly exceeds the $\pm$16 kW limit. In the APX + PS case only €328,- is earned, but the $\pm$16 kW limit is only exceeded in one time interval.

V. CONCLUSIONS & FUTURE WORK

In this work, a novel modular approach for control of an energy storage device, supporting simultaneously multiple objectives, is presented, referred to as *virtual battery* (control) setup. This control strategy incorporates existing battery models and control algorithms. This control strategy is tested using simulations of a 16 house neighbourhood. Results of the virtual battery setup are compared to results of a standard battery setup.

It is demonstrated that, as expected, the virtual battery setup performs in some cases significantly better than the standard battery setup. In particular, combining the goals *peak-shaving* and *grid balancing* lead to solutions with a grid friendly behaviour, i.e. the grid exchanges are minimised. Moreover, combining the goals *profiting on the APX market* and *peak-shaving* leads to significant financial benefits, while the grid exchange stays within the grid limitations.

In this work only simple cases using the virtual battery setup are discussed. Future work is dedicated to explore more elaborate cases, e.g. where $\sum_{i=1}^{n} C_i > C$ and/or where $n > 2$. Future work is also dedicated to the development of an algorithm to adapt and optimize the fractions of the ASD capacity dedicated to the different goals over time.

VI. ACKNOWLEDGEMENTS

This work is financially supported by the European Union and the European Fund for Regional Development (Project OP-Oost PROJ-00939). Furthermore, the authors thank *Egbert Bouwhuis* for providing the APX market dataset and the reviewers for their constructive comments on this work.

REFERENCES

[1] S. Nykamp, T. Knop, T. Rott, and K. Keller, "Forecast the grid oriented battery operation to enable a multi-use approach and discussion of the regulatory framework," in *Cired 24th International Conference on Electricity Distribution*, 2017.

[2] G. Gutermuth and M. Giuntoli, "Network operator owned storages as an option for congestion management," in *2020 IEEE PES Innovative Smart Grid Technologies Europe (ISGT-Europe)*, 2020, pp. 1074–1078.

[3] B. Homan, M. V. ten Kortenaar, J. L. Hurink, and G. J. M. Smit, "A realistic model for battery state of charge prediction in energy management simulation tools," *Energy*, vol. 171, pp. 205–217, 2019.

[4] K. S. Ng, C. S. Moo, Y. P. Chen, and Y. C. Hsieh, "Enhanced coulomb counting method for estimating SoC and SoH of Li-ion batteries," *Applied Energy*, vol. 86, no. 9, pp. 1506–1511, 2009.

[5] G. Hoogsteen, "A cyber-physical systems perspective on decentralized energy management," Ph.D. dissertation, University of Twente, 2017.

[6] B. Homan, G. Hoogsteen, S. Nebiolo, J. L. Hurink, and G. J. M. Smit, "Maximizing the degree of autarky of a 16 house neighbourhood by locally produced energy and smart control," *Sustainable Energy, Grids and Networks*, vol. 20, p. 100270, 2019.

[7] G. Hoogsteen, A. Molderink, J. L. Hurink, and G. J. M. Smit, "Generation of flexible domestic load profiles to evaluate demand side management approaches," in *IEEE Energycon 2016*, 2016, pp. 1–6.

[8] M. E. T. Gerards, H. A. Toersche, G. Hoogsteen, T. van der Klauw, J. L. Hurink, and G. J. M. Smit, "Demand side management using profile steering," in *IEEE Powertech 2015*, 2015, pp. 1–6.

[9] G. Hoogsteen, A. Molderink, J. L. Hurink, and G. J. M. Smit, "Asynchronous event driven distributed energy management using profile steering." in *IEEE Powertech 2017*, 2017, pp. 1–6.

[10] Tennet b.v., "APX passive imbalance market prices 1/1/2019 - 1/1/2021," [Online] Available: http://www.tennet.org.